

Inverse Design of Near-Field Transducer for Heat-Assisted Magnetic Recording Using Topology Optimization

Prabhu K. Venuthurumilli, Zhou Zeng, and Xianfan Xu 

School of Mechanical Engineering, Birck Nanotechnology Center, Purdue University, West Lafayette, IN 47907 USA

Heat-assisted magnetic recording (HAMR) is one of the next generation technologies in data storage that can increase the areal density to beyond 1.5 Tb/in². Near-field transducer (NFT) is a key component of the HAMR system that locally heats the recording medium by concentrating light below the diffraction limit using surface plasmons. In this work, we use density-based topology optimization for inverse design of NFT for a desired temperature profile in the recording medium. We first perform an inverse thermal calculation to obtain the required volumetric heat generation (electric field) for a desired temperature profile. Then an inverse electromagnetic design of NFT is performed for achieving the desired electric field. NFT designs for both generating a small heated spot size and a heated spot with desired aspect ratio in recording medium are demonstrated.

Index Terms—Heat-assisted magnetic recording (HAMR), near field transducer (NFT).

I. INTRODUCTION

THERE is always a need for increased storage capacity due to the increased amount of digital data. To meet this demand, the hard drive industry is pushing for higher areal density (bits per square inch) of hard drives [1]–[4]. The current recording technology of perpendicular magnetic recording is reaching its limit near 1.5 Tb/in² [5]. Further scaling down the grain volume of storage medium is not feasible due to the superparamagnetic limit ($K_u V/k_b T > 70$; where K_u is the magnetic anisotropy, V is the volume of the grain, k_b is the Boltzmann's constant, and T is the temperature) of the medium, i.e., the magnetic state becomes thermally unstable [4]. It is possible to further decrease the grain volume and keep it thermally stable with the use of large magnetic anisotropy materials including FePt [2]. However, the coercivity of these large anisotropy materials is greater than the magnetic field that can be generated with the current hard drive head technology. Heat-assisted magnetic recording (HAMR) is one of the possible technologies to address this issue, where the recording medium is heated beyond Curie point to reduce its coercivity during recording, which enables writing with the available amount of magnetic field in the recording head. It has been projected that the HAMR technology can achieve an areal density beyond 1.5 Tb/in² [5].

The primary goal of HAMR is to heat the recording medium locally (few 10 s of nm) which is much smaller compared with the diffraction limit of the light wavelength (800 nm) used in the HAMR system for heating the recording medium. HAMR system uses a metallic nano antenna/aperture also known as near field transducer (NFT), and locally heats by concentrating the light below the diffraction limit using surface plasmons [1].

Several NFT designs have been investigated including triangle antenna, E antenna, lollipop antenna, bowtie apertures, and C apertures [1], [2], [6]–[11]. Traditional design approaches use parameter sweep in optimizing the geometry of the design, i.e., highly constrained optimization without changing the topology in general.

In this work, we use topology optimization for inverse design of NFT for a desired temperature profile in the recording medium. With topology optimization, unexpected NFT topology may be produced which possibly gives an optimized solution that may not be obtained with intuition using a traditional parameter sweep of the design. Topology optimization has been used in various applications including improving coupling efficiency of nano-phonic grating coupler, localizing, and enhancing electromagnetic energy using Ag antenna-strip, designing waveguide for HAMR, designing the magnet for a desired magnetic field, maximizing bandgap in photonic crystals, designing nanostructures for extraordinary optical transmission, and surface plasmonic cloaking [12]–[17]. In this work, we first perform an inverse thermal calculation to obtain a required volumetric heat generation (electric field) in the recording medium for achieving a desired temperature profile. We use FePt as a recording medium and the curie point of FePt at 750 K [18]. We consider a targeted temperature rise of 450 K for 1 ns of heating in a desired heated region. We then perform an inverse electromagnetic field calculation for NFT design using topology optimization to generate a required electric field in the recording medium. This optimization is carried out by minimizing an objective function which is the difference between the electric field generated by the NFT and the targeted electric field in the recording medium, using a discrete adjoint method with finite-difference time-domain (FDTD) as a solver. Details of this method have been given in a previous work in which reconstructing the electric field of a plasmonic bowtie aperture has been demonstrated [19]. We use this inverse design procedure to find NFTs for producing different targeted rectangular heated spot size in the recording medium. We also attempt to find the smallest heated spot in the recording medium. The heated spot size and gradient along

Manuscript received December 23, 2020; revised March 6, 2021 and April 23, 2021; accepted June 9, 2021. Date of publication June 18, 2021; date of current version July 20, 2021. (Prabhu K. Venuthurumilli and Zhou Zeng contributed equally to this work.) Corresponding author: X. Xu (e-mail: xxu@ecn.purdue.edu).

Color versions of one or more figures in this article are available at <https://doi.org/10.1109/TMAG.2021.3090659>.

Digital Object Identifier 10.1109/TMAG.2021.3090659

0018-9464 © 2021 IEEE. Personal use is permitted, but republication/redistribution requires IEEE permission.
See <https://www.ieee.org/publications/rights/index.html> for more information.

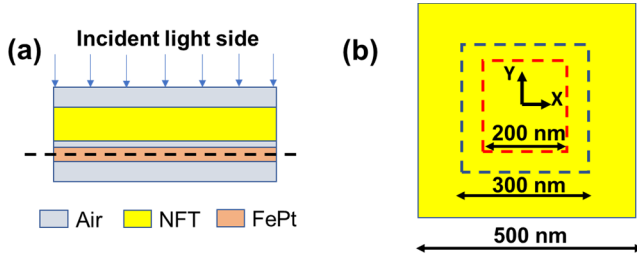


Fig. 1. Schematic of HAMR system considered in electromagnetic field simulation. (a) Side view; stack from incident light side: air, 60 nm-thick NFT (gold), 4 nm-thick air, 10 nm-thick FePt, air. (b) Top view showing the simulation domain of 500 nm \times 500 nm, the design region of NFT 200 nm \times 200 nm, and the field reconstructing region of 300 nm \times 300 nm at the mid plane in the FePt medium which is also shown by the dotted line in (a).

both the axes at 20 and 50 K below the maximum temperature rise of 450 K, and the required laser power for each design are compared.

II. DESCRIPTION OF THE SIMULATION MODELS

A. Inverse Thermal Design

We considered a single-layer recording medium with a simplified HAMR system, and the geometry of the simulation model is shown in Fig. 1. Fig. 1(a) shows the side view of the simulation model. It consists of air, the NFT, and the recording medium. The NFT is made of gold with a thickness of 60 nm and a recording medium is a 10 nm-thick FePt film. A 4 nm-thick air gap is considered between the NFT and FePt recording medium.

We perform the inverse thermal design by considering a 2-D FePt recording film, i.e., the temperature in the FePt is uniform in the thickness direction. The thermal properties of FePt are obtained from [20]. The vertical thermal conductivity of FePt is 7 W/mK which is five times more than that of lateral thermal conductivity of 1.5 W/mK. A 2-D thermal analysis (with lateral thermal conductivity) was considered in this work. The density \times specific heat of FePt used in the calculation is 3.2×10^6 J/m³K [20]. For an infinite 2-D space, the temperature rise can be obtained by the convolution product of the volumetric heat generation q and the Green's function G

$$\Delta T(r, t) = \frac{\alpha}{k} \int_0^t \int_{R^2} G(r - r', \tau) q(r') d^2 r' d\tau \quad (1)$$

where r is the coordinate vector and $G(r, \tau)$ is given by

$$G(r, \tau) = \frac{1}{4\pi\alpha t} e^{-\frac{|r|^2}{4\alpha t}}. \quad (2)$$

We intend to find a required volumetric heat source q that generates a uniform temperature profile within a given rectangular region in the recording medium after the medium is heated for 1 ns. The temperature rise in this region is 450 K. The volumetric heat generation to produce this temperature profile is obtained from the following optimiza-

tion/minimization calculation:

$$\begin{aligned} \min_q & 0.5 \iint_{r \in A} (\Delta T(r, t_o) - 450)^2 d^2 r \\ \text{s.t. } \Delta T(r, t) &= \frac{\alpha}{k} \int_0^t \int_{R^2} G(r - r', \tau) q(r') d^2 r' d\tau \\ &\text{and } q_l \leq q \leq q_u \end{aligned} \quad (3)$$

where q_l, q_u are the lower bound and the upper bound of the volumetric heat source. In our calculation, we use a nominal absorption $q_o = 2.77 \times 10^{18}$ W/m³ (a diode laser of 3 mW power, 300 nm beam waist, and 800 nm wavelength that is completely absorbed by the medium), and assign values to the lower bound and upper bound by $q_l = 0.008q_o$ and $q_u = 10q_o$. The lower bound is set to a very low value that does not have influence on the calculation results. The upper bound is found by trial and error as the maximum q found is about 3.62 q_o hence this upper bound is sufficient. We use the limited memory Broyden–Fletcher–Goldfarb–Shanno with bound constraints (L-BFGS-B) algorithm to solve the problem as a local gradient-based optimization [21].

Inverse thermal calculations are performed on a domain of 300 nm \times 300 nm, with a 2 nm grid size. A direct solution for the above optimization problem can produce very sharp peaks (with half width half maximum of ~ 1 nm) for the volumetric heat source q . We found that the electromagnetic optimization produces structures that do not have sharp peaks. Therefore, we can also impose a Gaussian filter function $w = e^{-\frac{|r|^2}{2a^2}}$ on the volumetric heat generation, $q_f = q * w$ to reduce the sharpness of the peaks and reduce computation time, where q_f is the filtered absorption and $*$ denotes convolution. We used a Gaussian filter of radius $a = 2$ nm. As a result, the final optimization is given by

$$\begin{aligned} \min_q & 0.5 \iint_{r \in A} (\Delta T(r, t_o) - 450)^2 d^2 r \\ \text{s.t. } \Delta T(r, t) &= \frac{\alpha}{k} \int_0^t \int_{R^2} G(r - r', \tau) q_f(r') d^2 r' d\tau \\ & q_l \leq q \leq q_u \text{ and } q_f = q * w. \end{aligned} \quad (4)$$

B. Inverse Electromagnetic Design

As shown in Fig. 1(a), a plane wave of wavelength 800 nm is incident from air onto NFT. The optical properties of air, gold, and FePt are taken from [20] and the optical properties used in the electromagnetic field simulations are given in Table 1.

The volumetric heat source due to absorption of electromagnetic energy is related to the electric field as

$$q = \frac{1}{2} \epsilon_o \omega \text{Im}(\epsilon) |E|^2 \quad (5)$$

where ϵ_o is the free-space permittivity, ω is the frequency of the light, $\text{Im}(\epsilon)$ is the imaginary part of the complex permittivity, and $|E|$ is the magnitude of the electric field.

We perform inverse electromagnetic design to obtain an NFT which generates a volumetric heat source [the electric field according to (5)] in the recording medium that is obtained from the inverse thermal calculation. The top view of the simulation domain is shown in Fig. 1(b) with

TABLE I
OPTICAL PROPERTIES USED IN ELECTROMAGNETIC FIELD SIMULATIONS

	n	k
Air	1	0
NFT - Au	0.21	4.73
Storage medium - FePt	3.2	2.6

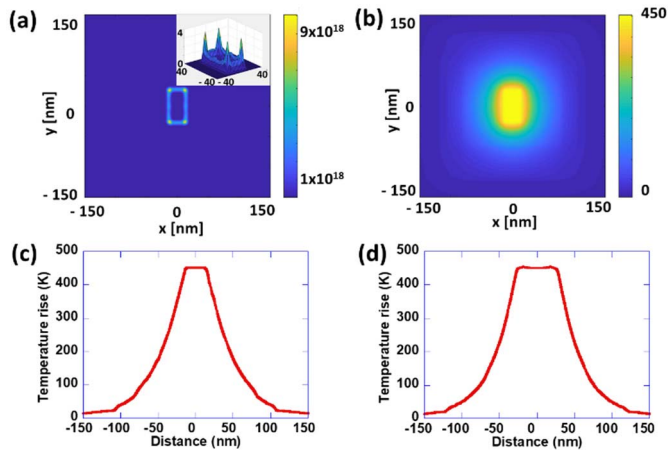


Fig. 2. Inverse thermal calculation for generating a $30 \text{ nm} \times 60 \text{ nm}$ heat spot. (a) Obtained volumetric heat generation (W/m^3). The inset shows the isometric view of the normalized volumetric heat generation. (b) Temperature rise (K) in the recording medium with the volumetric heat generation in Fig. 2(a). (c) Temperature rise along the x -axis in Fig. 2(b). (d) Temperature rise along y -axis in Fig. 2(b).

a size of $500 \text{ nm} \times 500 \text{ nm}$, and the field reconstruction area is of $300 \text{ nm} \times 300 \text{ nm}$ at the mid plane of the FePt recording medium as shown by the dotted line in Fig. 1(a). The design region of NFT is limited to an area of $200 \text{ nm} \times 200 \text{ nm}$ i.e., the region where the density can vary between 1 and 0, where 1 represents gold and 0 represents air (aperture). The polarization of the light is in the x -direction [the horizontal direction in Fig. 1(b)].

We used the same method as in our previous work of inverse design for reconstructing the electric field of a plasmonic bowtie aperture based on topology optimization [19]. The objective function of the optimization is to minimize the difference between the electric field E and the desired electric field E_0 on the field reconstruction surface S . We used a density-based topology optimization with non-linear material interpolation. As a result, we solve the following optimization problem:

$$\min_{\rho} F(E) = \int_S (|E| - |E_0|)^2 dS. \quad (6)$$

In our calculation, density-based topology optimization based on a discrete adjoint method with FDTD is used in inverse electromagnetic design to guarantee the exactness of

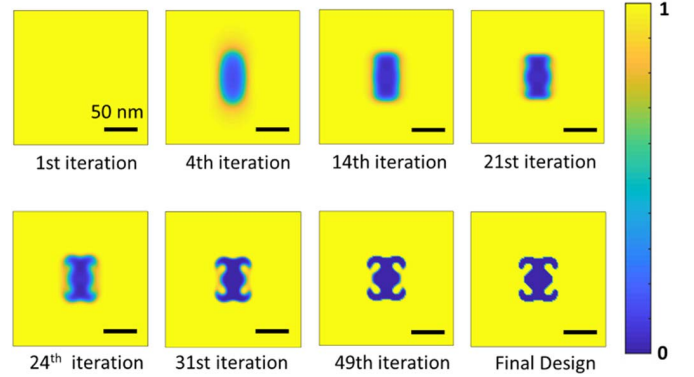


Fig. 3. Density evolution of NFT and the final NFT design for generating a targeted heated spot of $30 \text{ nm} \times 60 \text{ nm}$ in the recording medium. Density 1 represents gold and 0 represents air (aperture). All scale bars are 50 nm.

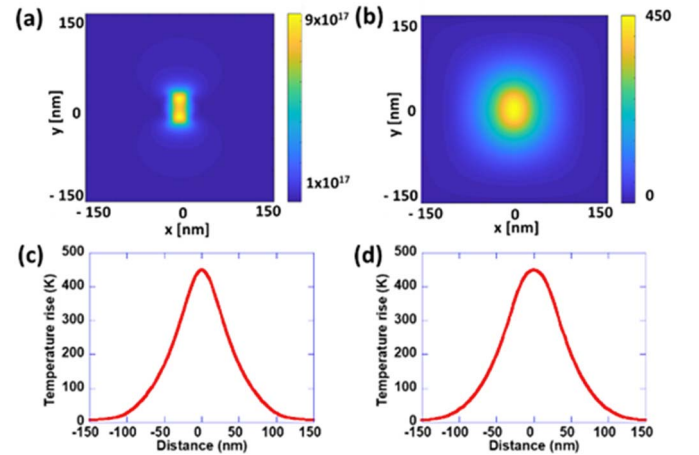


Fig. 4. Thermal calculations with the obtained NFT design for the targeted heated spot of $30 \text{ nm} \times 60 \text{ nm}$. (a) Volumetric heat generation (W/m^3) in the recording medium with the obtained NFT design. (b) Scaled temperature rise (K) of recording medium with the obtained NFT design. (c) Temperature rise along the x -axis in Fig. 4(b). (d) Temperature rise along y -axis in Fig. 4(b).

gradient calculation. The optimization algorithm starts with density 1 in the design region and is solved iteratively to minimize the objective function. The final design has the density of either 1 or 0 but not the intermediate values. Details of the inverse calculations are given in [19].

Once the inverse designs are completed, we use the ANSYS Workbench with the NFT design obtained in topology optimization to compute the electric field, which is then used to calculate the temperature rise of the recording medium after 1 ns of heating using (1).

III. RESULTS AND DISCUSSION

A. Inverse Thermal Calculation for Generating a Heat Spot of $30 \text{ nm} \times 60 \text{ nm}$ in Recording Medium

We first show the result of the inverse thermal calculation for generating a rectangular heated spot of $30 \text{ nm} \times 60 \text{ nm}$ in the recording medium, i.e., a temperature rise of 450 K in that region after 1 ns of heating. The use of a size of $30 \text{ nm} \times 60 \text{ nm}$ or an aspect ratio of 1:2 is due to the

TABLE II
HEATED SPOT SIZE AND GRADIENT ALONG BOTH THE AXES AT 430 AND 400 K, WITH DIFFERENT RECTANGULAR TARGETED HEATED SPOT SIZE, AND THE CORRESPONDING POWER REQUIRED FOR PEAK TEMPERATURE RISE OF 450 K

Target Heat spot size (nm x nm)	Area (nm x nm)		Gradient (K/nm)				Power (mW)
			X - axis		Y - axis		
	At 430 K	At 400 K	At 430 K	At 400 K	At 430 K	At 400 K	
30 x 60	17.4 x 24.7	28.6 x 38.2	4.5	3.6	6.4	5.4	3.2
25 x 50	16.5 x 22.6	27.0 x 35.4	5.0	3.5	6.5	5.5	6.6
20 x 40	14.5 x 19.4	24.2 x 31.4	5.1	3.7	7.4	5.8	8.8
15 x 30	14.0 x 18.4	23.5 x 29.8	5.2	4.1	7.0	6.3	10.2
10 x 20	14.0 x 17.7	23.6 x 29.0	5.1	4.3	6.9	6.5	7.4
8 x 16	13.7 x 17.0	23.0 x 27.6	5.5	4.8	7.1	6.5	9.3

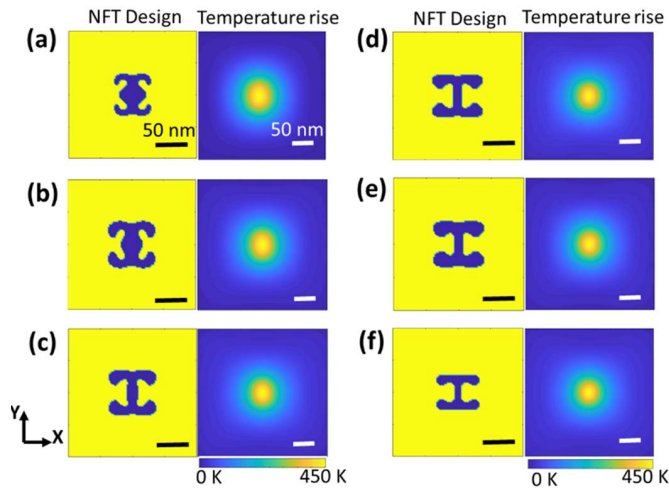



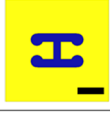



Fig. 5. Generating smaller heated spot in the recording medium, with different targeted heated spot size of (a) 30 nm × 60 nm, (b) 25 nm × 50 nm, (c) 20 nm × 40 nm, (d) 15 nm × 30 nm, (e) 10 nm × 20 nm, and (f) 8 nm × 16 nm. The obtained designs of NFTs are shown on the left and the scaled temperature rises in the recording medium are shown on the right for each case. All scale bars are 50 nm.

elongated geometry of a storage unit in a hard disk drive. The inverse thermal calculation results are shown in Fig. 2. Fig. 2(a) shows the obtained volumetric heat generation profile for generating the heated spot of 30 nm × 60 nm. From Fig. 2(a) we observe that the volumetric heat generation profile has four hot spots at four corners and also has heat generation along the edges to produce a desired temperature rise. The inset in Fig. 2(a) shows the isometric view of the normalized volumetric heat generation. Using this volumetric heat generation profile, the corresponding temperature rise in the recording medium is calculated using (1) and is shown in Fig. 2(b). The line profiles along x - and y -axes

TABLE III
EFFECT OF CURVATURE IN NFT. ALL SCALE BARS ARE 50 NM

Case	Area (nm ²)	
	At 430 K	At 400 K
	14.0 x 17.7	23.6 x 29.0
	15.0 x 18.7	25.1 x 30.4
	15.3 x 18.8	25.5 x 30.3
	15.7 x 19.3	26.3 x 31.1
	15.7 x 19.3	26.3 x 31.2

of the temperature rise are shown in Fig. 2(c) and (d). From Fig. 2(b) to (d), we can see the temperature rise of 450 K in the rectangular region of 30 nm × 60 nm. However, it should be noted that there are finite temperature gradients around the heated region, compared with the steep rise (infinitely large temperature gradient) of the temperature to 450 K in the desired temperature profile. The heat diffusion within the

TABLE IV

HEATED SPOT SIZE AND GRADIENT ALONG BOTH THE AXES AT 430 AND 400 K, WITH DIFFERENT TARGETED HEATED SPOT SIZE FOR GENERATING HIGH ASPECT RATIO HEATED SPOT IN THE RECORDING MEDIUM, AND THE CORRESPONDING POWER REQUIRED FOR PEAK TEMPERATURE RISE OF 450 K

Target Heat spot size (nm x nm)	Area (nm x nm)		Gradient (K/nm)				Power (mW)
			X - axis	Y - axis	X - axis	Y - axis	
	At 430 K	At 400 K	At 430 K	At 400 K	At 430 K	At 400 K	
10 x 20	14.0 x 17.7	23.6 x 29.0	5.1	4.3	6.9	6.5	7.4
10 x 30	14.1 x 18.4	23.5 x 29.8	5.3	4.1	7.0	6.3	8.0
10 x 40	14.4 x 20.3	24.1 x 32.6	5.0	4.2	7.3	6.1	8.7
10 x 60	14.6 x 22.5	24.4 x 36.2	5.0	3.4	7.2	5.5	8.2
10 x 80	14.9 x 26.8	25.0 x 42.9	4.7	2.8	6.9	4.5	7.8
10 x 100	15.9 x 34.9	26.2 x 54.4	4.3	2.3	6.6	3.8	8.4

1 ns heating time causes such a temperature gradient, which is not possible to be avoided.

B. Inverse Electromagnetic Field Calculation for Generating a Heated Spot of 30 nm × 60 nm in the Recording Medium

With the obtained volumetric heat generation in Fig. 2(a), we calculate the required electric field at mid plane of FePt using (5). The topology optimization of NFT design is then performed to achieve this required electric field. The final NFT design from topology optimization as well as the density evolution during the optimization process is shown in Fig. 3, where density 1 represents gold and 0 represents air (aperture). The blue region in the final NFT design indicates the aperture in the NFT.

The obtained NFT is then used to compute the electric field distribution using ANSYS HFSS and temperature distribution using (1) and the results are shown in Fig. 4. The volumetric heat source in the recording medium produced by the NFT is shown in Fig. 4(a). It is noticed that the NFT does not produce the exact targeted electric field distribution, and the difference with the targeted volumetric heat generation can be seen by comparing with Fig. 2(a). In other words, the desired volumetric heat generation or electric field with four sharp corners shown in Fig. 2(a) cannot be obtained exactly, rather, the designed NFT produces an electric field that minimizes the objective function in (6). The calculated temperature rise, with the maximum temperature rise scaled to 450 K, is shown in Fig. 4(b), and the line profiles along x - and y -axes of the temperature rise are shown in Fig. 4(c) and (d). It is seen that heated spot size is about ~ 29 nm × 39 nm at 50 K below the maximum temperature. This heat spot size is obtained by the contour at 400 K temperature rise. This heated spot size is close to the desired heated spot size along the x -axis, but is reduced along the y -axis compared with the desired size.

The reduction of the size along one direction and the resulting change in the aspect ratio will be further analyzed later.

C. Generating Smallest Heated Spot in the Recording Medium

In order to find the smallest heated spot in the recording medium, we performed topology optimization of NFTs to achieve rectangular heated spot size of 30 nm × 60 nm, 25 nm × 50 nm, 20 nm × 40 nm, 15 nm × 30 nm, 10 nm × 20 nm, and 8 nm × 16 nm. The obtained NFT designs and the corresponding scaled temperature rises in the recording medium are shown in Fig. 5. The heated spot sizes obtained by the contours and gradient along both the axes at 20 and 50 K below the maximum temperature rise of 450 K, and the required laser power for each design are summarized in Table 2. We find that the minimum spot size is about ~ 14 nm × 17 nm at 20 K below the maximum temperature, and is about 23 nm × 29 nm at 50 K below the maximum temperature despite the targeted sizes of 15 nm × 30 nm, 10 nm × 20 nm, and 8 nm × 16 nm. This indicates the minimum spot size that can be achieved. On the other hand, the achieved aspect ratio at minimum spot size is less than 2.

However, we would like to note that a simplified HAMR model was used to demonstrate the inverse design of NFT using topology optimization. Using the multilayer stack of the substrate [20] with a heat sink, the same NFT design will give a smaller heat spot size, especially along the x -direction (about four times) and high gradients (four times) as compared with the simplified model.

An obvious observation is that the geometries of NFT obtained by the topology optimization are intricate. We study the effect of the curvatures of the NFT geometry obtained with a targeted heat spot size of 10 nm × 20 nm, by performing direct calculations by modifying/removing (some of) the curvatures in NFT. Table 3 presents the modified NFTs and the

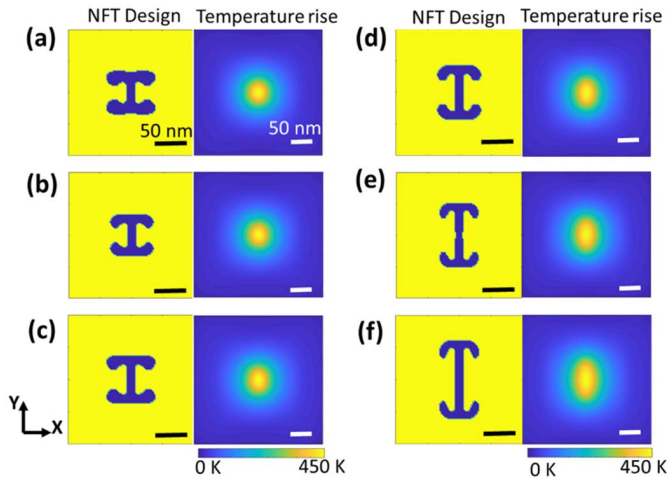


Fig. 6. Generating high aspect ratio heated spot in the recording medium, with different targeted heated spot size of (a) $10 \text{ nm} \times 20 \text{ nm}$, (b) $10 \text{ nm} \times 30 \text{ nm}$, (c) $10 \text{ nm} \times 40 \text{ nm}$, (d) $10 \text{ nm} \times 60 \text{ nm}$, (e) $10 \text{ nm} \times 80 \text{ nm}$, and (f) $10 \text{ nm} \times 100 \text{ nm}$. The obtained designs of NFT are shown on the left and the scaled temperature rise in the recording medium are shown on the right for each case. All scale bars are 50 nm.

resulting size of the heated spot at 430 and 400 K temperature rise. We observe that the heated spot size is smallest from the inverse designed NFT.

D. Generating Heated Spot With Higher Aspect Ratio

As discussed earlier when the targeted heat spot size is small, the obtained heated spot has an aspect ratio less than 2. Here we investigate if we can achieve an aspect ratio 2 by increasing the targeted aspect ratio. We performed topology optimization for targeted heat spot size of $10 \text{ nm} \times 30 \text{ nm}$, $10 \text{ nm} \times 40 \text{ nm}$, $10 \text{ nm} \times 60 \text{ nm}$, $10 \text{ nm} \times 80 \text{ nm}$, and $10 \text{ nm} \times 100 \text{ nm}$. The obtained NFT designs and the corresponding temperature rises in the recording medium are shown in Fig. 6. We can see that the aspect ratio of obtained heated spot size increases with the increase of the targeted aspect ratio. The heated spot sizes and gradient along both the axes at 20 and 50 K below the maximum temperature rise of 450 K, and the required laser power for each design are given in Table 4. It is seen that with the targeted heat spot size of $10 \text{ nm} \times 80 \text{ nm}$ and $10 \text{ nm} \times 100 \text{ nm}$, an aspect ratio 2 can be obtained in the recording medium.

IV. CONCLUSION

In summary, we demonstrate using an inverse design process to design NFTs to obtain targeted heated spot size in the recording medium for heat-assisted magnetic recording. Inverse thermal calculation is first performed to obtain the desired volumetric heat generation (electric field) in the recording medium. Then the inverse electromagnetic field calculation is performed to obtain an NFT that produces the desired electric field. NFT designs for generating a smallest heated spot is carried out, which is found to be $\sim 14 \text{ nm} \times 17 \text{ nm}$ at 430 K temperature rise, or 20 K below the peak temperature. It is also shown that the obtained NFTs are able to produce a smaller heated spot compared with NFTs

for which the intricate curvatures are removed. A desired aspect ratio of 2 can be obtained by initially selecting a higher targeted aspect ratio. This work indicates that inverse design can be used to obtain NFTs with desired requirements, and to produce NFT structures that are not intuitively considered, thus possibly open up more design options of NFT.

ACKNOWLEDGMENT

This work was supported by ASTC—the Advanced Storage Technology Consortium.

REFERENCES

- [1] B. C. Stipe *et al.*, “Magnetic recording at 1.5 Pbm^{-2} using an integrated plasmonic antenna,” *Nature Photon.*, vol. 4, no. 7, pp. 484–488, 2010.
- [2] W. A. Challener *et al.*, “Heat-assisted magnetic recording by a near-field transducer with efficient optical energy transfer,” *Nature Photon.*, vol. 3, no. 4, pp. 220–224, Apr. 2009.
- [3] L. Pan and D. B. Bogy, “Heat-assisted magnetic recording,” *Nature Photon.*, vol. 3, no. 4, pp. 2–3, 2009.
- [4] N. Zhou *et al.*, “Plasmonic near-field transducer for heat-assisted magnetic recording,” *Nanophotonics*, vol. 3, no. 3, pp. 141–155, Jun. 2014.
- [5] M. T. Kief and R. H. Victora, “Materials for heat-assisted magnetic recording,” *MRS Bull.*, vol. 43, no. 2, pp. 87–92, Feb. 2018.
- [6] W. A. Challener and A. V. Itagi, “Near-field optics for heat-assisted magnetic recording (experiment, theory, and modeling),” in *Modern Aspects of Electrochemistry*. New York, NY, USA: Springer, 2009, pp. 53–111.
- [7] N. Zhou, L. M. Traverso, and X. Xu, “Power delivery and self-heating in nanoscale near field transducer for heat-assisted magnetic recording,” *Nanotechnology*, vol. 26, no. 13, Mar. 2015, Art. no. 134001.
- [8] N. Zhou, E. C. Kinzel, and X. Xu, “Nanoscale ridge aperture as near-field transducer for heat-assisted magnetic recording,” *Appl. Opt.*, vol. 50, no. 31, pp. G42–G46, 2011.
- [9] X. Shi and L. Hesselink, “Mechanisms for enhancing power throughput from planar nano-apertures for near-field optical data storage,” *Jpn. J. Appl. Phys.*, vol. 41, no. 3B, pp. 1632–1635, Mar. 2002.
- [10] A. Datta and X. Xu, “Comparative study of optical near-field transducers for heat-assisted magnetic recording,” *Opt. Eng.*, vol. 56, no. 12, May 2017, Art. no. 121906.
- [11] N. Abadía *et al.*, “Optical and thermal analysis of the light-heat conversion process employing an antenna-based hybrid plasmonic waveguide for HAMR,” *Opt. Exp.*, vol. 26, no. 2, pp. 1752–1765, 2018.
- [12] J. Andkjær, S. Nishiwaki, T. Nomura, and O. Sigmund, “Topology optimization of grating couplers for the efficient excitation of surface plasmons,” *J. Opt. Soc. Amer. B, Opt. Phys.*, vol. 27, no. 9, pp. 1828–1832, 2010.
- [13] R. E. Christiansen, J. Vester-Petersen, S. P. Madsen, and O. Sigmund, “A non-linear material interpolation for design of metallic nano-particles using topology optimization,” *Comput. Methods Appl. Mech. Eng.*, vol. 343, pp. 23–39, Jan. 2019.
- [14] S. Bhargava and E. Yablonovitch, “Lowering HAMR near-field transducer temperature via inverse electromagnetic design,” *IEEE Trans. Magn.*, vol. 51, no. 4, pp. 1–7, Apr. 2015.
- [15] C. Huber *et al.*, “Topology optimized and 3D printed polymer-bonded permanent magnets for a predefined external field,” *J. Appl. Phys.*, vol. 122, no. 5, Aug. 2017, Art. no. 053904.
- [16] J. S. Jensen and O. Sigmund, “Topology optimization for nanophotonics,” *Laser Photon. Rev.*, vol. 5, no. 2, pp. 308–321, Mar. 2011.
- [17] Y. Deng, Z. Liu, C. Song, J. Wu, Y. Liu, and Y. Wu, “Topology optimization-based computational design methodology for surface plasmon polaritons,” *Plasmonics*, vol. 10, no. 3, pp. 569–583, Jun. 2015.
- [18] C.-B. Rong *et al.*, “Size-dependent chemical and magnetic ordering in $\text{L}_{10}\text{-FePt}$ nanoparticles,” *Adv. Mater.*, vol. 18, no. 22, pp. 2984–2988, Nov. 2006.
- [19] Z. Zeng, P. K. Venuthurumilli, and X. Xu, “Inverse design of plasmonic structures with FDTD,” *ACS Photon.*, vol. 8, no. 5, pp. 1489–1496, May 2021.
- [20] A. Datta and X. Xu, “Infrared near-field transducer for heat-assisted magnetic recording,” *IEEE Trans. Magn.*, vol. 53, no. 12, pp. 1–5, Dec. 2017.
- [21] R. H. Byrd, P. Lu, J. Nocedal, and C. Zhu, “A limited memory algorithm for bound constrained optimization,” *SIAM J. Sci. Comput.*, vol. 16, no. 5, pp. 1190–1208, Sep. 1995.